sciendo

Journal of Electrical Engineering, Vol. 76, No. 4, 2025, pp. 361-369

Robust fixed-time control for DC-DC converter with matched and mismatched perturbations

Varin Cholahan, Worapong Tangsrirat

This paper introduces a state-dependent variable exponent coefficient for fixed-time sliding mode control. The proposed state-dependent sliding surface ensures system stability and facilitates a rapid response within a fixed timeframe, while also addressing both matched and mismatched perturbations. This sliding mode control is applied to the DC-DC converter, a system that frequently encounters mismatched issues. By using the fixed-time concept, the designed sliding mode surface exhibits robustness, enabling it to manage both matched and mismatched perturbations within a fixed-time duration. We first present the average mathematical model for the continuous mode DC-DC converter. Next, a state-dependent sliding surface with a variable exponent coefficient is developed. Following next, the controller is designed to regulate the converter's voltage while effectively rejecting both matched and mismatched disturbances. The stability of the proposed approach is evaluated through the use of a Lyapunov function. Lastly, numerical simulations demonstrate rapid convergence and significant robustness against uncertainties in parameters, both matched and mismatched. When compared to other fixed-time and finite-time schemes, the proposed fixed-time controller is notable for its high efficiency and relatively straightforward control solution.

Keywords: DC-DC converter, fixed-time control, sliding mode control, state-dependent sliding surface, nonlinear control, mismatched parameter

1 Introduction

The DC-DC converter is widely utilized to stabilize the desired voltage output, which can be influenced by fluctuating conditions, nonlinearity, uncertainties, disturbances, and noise. The reliability of power during the conversion process is strongly dependent on the reliable operation of the power converter and its control mechanisms. A comprehensive review of the work in [1] provides essential insights into the classification of power converters and their corresponding control methods for various applications. The review indicates that numerous conventional converters and control strategies face various limitations in practical use, highlighting the necessity to thoroughly evaluate their effectiveness in specific systems. The buck converter is recognized as one of the simplest and most efficient power converters, capable of converting a higher DC voltage into a lower one. Its applications are varied, including micro-grids, renewable energy systems, photovoltaic configurations, battery charging, LED drivers, energy management, and speed control for both DC and AC motor drivers, among others. The proportional-integral-derivative (PID) control method is commonly utilized for DC-DC converters; however, it requires system linearization, which makes it more sensitive to external changes and uncertainties. Such issues present challenges for traditional linear regulators.

To address this challenge, a variety of non-linear control methods with a particular focus on sliding mode control (SMC) are employed. A detailed examination of SMC, which emphasizes notable progress and investigates emerging trends and challenges in its application within power electronics, can be found in [2]. The concept of a fixed-time control system was later introduced in [3] and has since been further developed through numerous studies. In 2021, a robust variable exponent coefficient fixed-time SMC approach was presented [4]. This innovative variable exponent sliding mode strategy is simple to implement, non-singular, and robust against both matched and mismatched disturbances, while remaining independent of initial conditions. Owing to the difficulties in accurately determining disturbance values in practical applications, the gain of the sliding mode controller often exceeds the upper threshold of lumped disturbances to ensure robustness and reduce chattering problems. To overcome this problem, observer-based controllers have demonstrated effectiveness in reducing the effects of unexpected external disturbances, uncertainties in the model, and excessive chattering within control systems. An integrated sliding mode controller utilizing an early-aged extended state observer was described in [5]. The adaptive terminal SMC strategy, along with the continuous fast terminal SMC was introduced in [6-7]. In [8], a super-twisting sliding-mode observer technique was also proposed. A sliding mode observer was employed to estimate the lump disturbances of PMSM in [9].

There are a significant number of research studies focused on mismatch problems. Researchers have proposed various schemes, such as LMI-based SMC in [10]

School of Engineering, King Mongkut's Institute of Technology Ladkrabang (KMITL), Bangkok 10520, Thailand
varin.chol@gmail.ac.th, worapong.ta@kmitl.ac.th

https://doi.org/10.2478/jee-2025-0037, Print (till 2015) ISSN 1335-3632, On-line ISSN 1339-309X

and adaptive-based SMC in [11]. The modified SMC scheme requires the mismatch disturbance to satisfy the bounded assumption of the H_2 norm with mismatch disturbance as the non-vanishing uncertainty described by [12]. In recent years, DOB-based SMC approaches have been introduced to address mismatch disturbances. These methods relax the unreasonable H_2 norm-bounded assumption and maintain the stable performance. In [13], an adaptive fixed-time disturbance observer-based (DOB) controller was proposed to mitigate the mismatch disturbance. Subsequently, an extended state observer-based sliding mode control (SMC) method was introduced to address the mismatch disturbance observed in the buck converter application in [14]. The findings from the previous research were further developed into finite-time control in [15].

Previous research has addressed control issues involving both matched and mismatched disturbances by employing observers. Few fixed-time controllers have been proposed in academic research to solve the issue of mismatched disturbances in DC-DC buck converters. Therefore, this research is among the first to introduce a fixed-time controller utilizing a chosen sliding surface to suppress mismatched disturbances. This article introduces an approach known as variable exponent fixed-time sliding mode, based on [4], to reduce both types of disturbances without the use of observers. This work demonstrates that the DC-DC buck converter efficiently regulates DC voltage, successfully achieving the desired output voltage through the application of a fixed-time control strategy. The results indicate that fixed-time control theory provides a robust foundation for developing control laws. This proposed fixed-time approach is based on variable exponent coefficients.

This study is organized as follows. Section 2 provides an overview of the average dynamic model for a DC-DC converter. Section 3 details the theory of a fixed-time control and state-dependent sliding surface, as well as the proposition to solve mismatched parameters. Section 4 demonstrates a DC-DC converter with both matched and mismatched perturbations. In Section 5, the fixed-time controller is designed. Stability proof is also derived in Section 6. Section 7 presents the simulation results of the proposed controller, comparing its performance with other methods. Finally, Section 8 summarizes the findings related to the state-dependent controller.

2 Average state-space model of DC-DC converter

When a power supply needs to work with a wide range of voltages, such as in an adjustable switch-mode power supply, and the load is sufficiently high, the DC-DC converter can be characterized as operating in continuous conduction mode (CCM). Additionally, for the purposes of advanced control, the converter may also be represented in discontinuous conduction mode (DCM) or composition mode. The conventional DC-DC converter depicted in Fig. 1 is widely utilized and has received significant attention in research studies. The converter is assumed to operate in DCM, as illustrated in Fig. 2, which can be classified into three separate regions. The fundamental operation of the buck converter can be described through the linear ordinary differential Eqns. (1), which are categorized as a non-smooth equation with a variable structure utilizing switching functions [16]:

$$\dot{v}_C = u_2\left(\frac{i_L}{C}\right) - \frac{v_C}{RC}, \tag{1a}$$

and

$$\dot{i}_L = u_2\left(\frac{u_1 v_{in} - v_C}{L}\right). \tag{1b}$$

The variable u_1 equals "1" when the switch is in the "on" position and equals "0" when the switch is "off". The switching function of u_2 = sgn[sgn(v_C) + sgn(i_L)] indicates that the status of the inductor determines the conduction mode of the converter, with v_C representing the voltage across the capacitor and i_L indicating the current flowing through the conductor. To limit the operational frequency, a common method is to utilize pulse width modulation (PWM), which is characterized by a constant switching period, T_s. The modulation duty cycle d serves as the control parameter in the state-space average dynamic model, representing the proportion of the period in which the switch remains in the "on" position. Furthermore, PWM effectively adjusts the output voltage, $v_C \in [0, v_{in}]$.

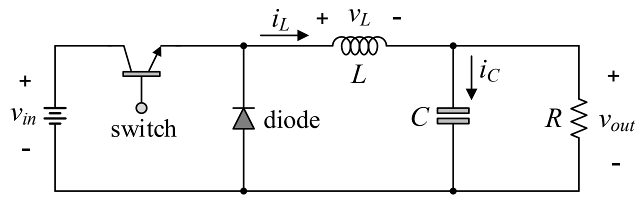

Fig. 1. Conventional DC-DC converter

According to Fig. 2, the operation regions of the DC-DC converter can be characterized by the following three state-space models:

1) CCM region I, when $u_2 = 1$ and $u_1 = 1$

$$A_1 = \begin{bmatrix} -\frac{1}{RC} & \frac{1}{C} \\ -\frac{1}{L} & 0 \end{bmatrix} \quad B_1 = \begin{bmatrix} 0 \\ \frac{1}{L} \end{bmatrix} \quad C_1 = \begin{bmatrix} 1 & 0 \end{bmatrix} \quad D_1 = 0 \tag{2}$$

2) DCM region II, when $u_2 = 0$

$$A_2 = \begin{bmatrix} -\dfrac{1}{RC} & 0 \\ 0 & 0 \end{bmatrix} \quad B_2 = \begin{bmatrix} 0 \\ 0 \end{bmatrix} \quad C_2 = \begin{bmatrix} 1 & 0 \end{bmatrix} \quad D_2 = 0 \qquad (3)$$

3) CCM region III, when $u_2 = 1$ and $u_1 = 0$

$$A_3 = \begin{bmatrix} -\dfrac{1}{RC} & \dfrac{1}{C} \\ -\dfrac{1}{L} & 0 \end{bmatrix} \quad B_3 = \begin{bmatrix} 0 \\ 0 \end{bmatrix} \quad C_3 = \begin{bmatrix} 1 & 0 \end{bmatrix} \quad D_3 = 0 \qquad (4)$$

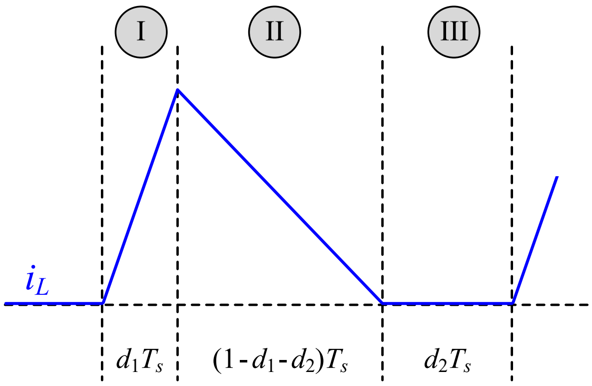

Fig. 2. Operation regions of the DC-DC converter

Using Eqn. (1), one can derive the average dynamic model of the CCM by:

$$\begin{aligned} A_{CCM} &= dA_1 + (1-d)A_3 \\ B_{CCM} &= dB_1 + (1-d)B_3 \\ C_{CCM} &= dC_1 + (1-d)C_3 \\ D_{CCM} &= dD_1 + (1-d)D_3 \end{aligned} \qquad (5)$$

where d is the duty cycle of the pulse width modulation circuit.

Since the duty cycle modulation serves as an input for the state, this leads to

$$\begin{bmatrix} \dot{\overline{v}}_C \\ \dot{\overline{i}}_L \end{bmatrix} = \begin{bmatrix} -\dfrac{1}{RC} & \dfrac{1}{C} \\ -\dfrac{1}{L} & 0 \end{bmatrix} \begin{bmatrix} \overline{v}_C \\ \overline{i}_L \end{bmatrix} + \begin{bmatrix} 0 \\ \dfrac{v_{in}}{L} \end{bmatrix} d \qquad (6)$$

Figure 3 shows the block diagram for the feedback control of a DC-DC converter. The controller compares the reference voltage v_r with the feedback voltage $\overline{v}_C(t)$ and uses this information to inform its actions. It employs fixed-time stabilization and generates a duty cycle command d that regulates the gate in the PWM circuit, thereby controlling the output voltage $\overline{v}_C(t)$ of the DC-DC converter.

3 Robust fixed-time stability and state dependent sliding surface

The representation of the dynamic equation is as follows:

$$\dot{x}(t) = g\left[x(t)\right],\ x(t) \in R^n, \text{ and } x(0) = x_0, \qquad (7)$$

where $x = (x_1, x_2) \in R^2$ and g denotes a continuous function characterized by the equilibrium condition $g(0) = 0$.

Theorem 1: [3] A Lyapunov candidate function exists that is continuous, differentiable, positive definite, and radially unbounded V: $R^n \to R^+$, such that

$$\dot{V}(x) \le -a_1 V(x)^{\kappa} - a_2 V(x)^{\varphi_v}, \qquad (8)$$

where $0 < \varphi_v < 1 < \kappa$, $x \in R^n$, $a_1 > 0$, and $a_2 > 0$. The settling function (T) is represented as

$$T(x_0) \le \frac{1}{a_1(1-\varphi_v)} + \frac{1}{a_2(\kappa - 1)}. \qquad (9)$$

The stability of the robust variable exponent coefficient over a fixed time concept is described in the following:

Theorem 2: [17] The dynamical system defined by the state-dependent exponent coefficient can be characterized as

$$\dot{x} = -c\left|x(t)\right|^{\frac{\eta x(t)^2}{1+\upsilon x(t)^2}} \operatorname{sgn}\left[x(t)\right] + \delta(t),$$

and $x(0) = x_0$, (10)

where $x(t) \in R$, $\eta > 0$, $\upsilon > 0$, and $\theta = \frac{\eta}{\upsilon+1} > 1$. In this case, the lumped disturbance $\left|\delta(t)\right|$ is positive bounded by constant ς. For the given $\varsigma > 0$ and $c > \varsigma e^{\frac{\eta}{2e}}$, the following describes the function T of the state-dependent system expressed in Eqn. (10).

$$T(x_0) \le \frac{1}{(c-\varsigma)(\theta-1)} + \frac{1}{\left(ce^{\frac{-\eta}{2e}} - \varsigma\right)}. \qquad (11)$$

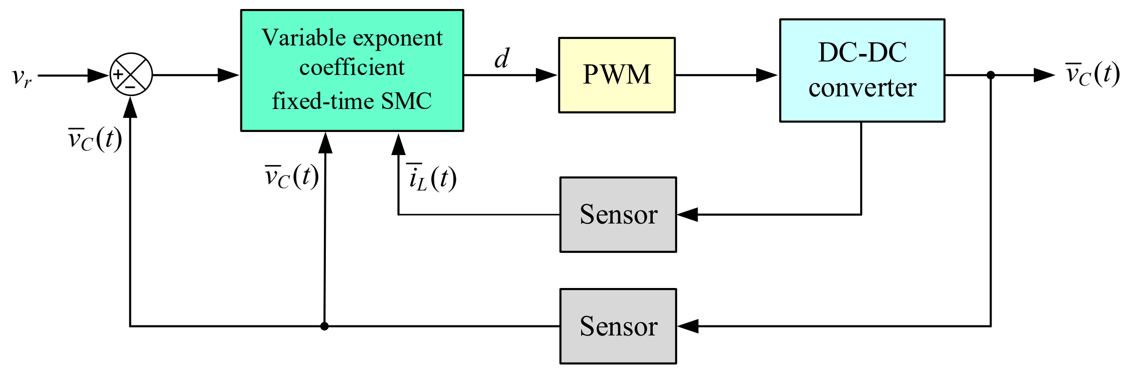

Fig. 3. Closed-loop control diagram of the DC-DC converter

***Proof*:** Consider the Lyapunov function expressed below:

$$V(x) = x^2 . \tag{12}$$

To achieve the desired outcome along the trajectory (10), the derivative of Eqn. (12) indicates that

$$\dot{V}(x) = -2c|x|^{\frac{\eta x^2}{1+\upsilon x^2}+1} + 2\varsigma x . \tag{13}$$

Considering the first case $V(x) > 1$, we have $\left(\frac{\eta x^2}{1+\upsilon x^2}+1\right) \ge \left(\frac{\eta}{1+\upsilon}+1\right) > 2$. As $|x| \ge 1$ and $\theta = \frac{\eta}{1+\upsilon} > 1$, Eqn. (13) might be rewritten to

$$\begin{aligned}\dot{V}(x) &\le -2(c-\varsigma)|x|^{\theta+1} \\ &\le -2(c-\varsigma)V(x)^{\frac{\theta+1}{2}}\end{aligned} . \tag{14}$$

As for $(c - \varsigma) > 0$ and $\frac{\theta+1}{2} > 1$, this ensures that the dynamical system described in Eqn. (10) with any initial condition $V(x) > 1$ reaches the sliding mode $V(x) \le 1$ within a fixed period of time $T_1 \le \frac{1}{(c-\varsigma)(\theta-1)}$.

In the second case, where $V(x) \le 1$, Eqn. (13) is rearranged as follows:

$$\dot{V}(x) = -2c|x||x|^{\frac{\eta x^2}{1+\upsilon x^2}} + 2\varsigma x . \tag{15}$$

As $\left(1+\upsilon x^2\right) \ge 1$ and $|x| \le 1$, the state dependent function is simplified to $\min\left(|x|^{\frac{\eta x^2}{1+\upsilon x^2}}\right) \ge \min\left(|x|^{\eta x^2}\right) = e^{\frac{-\eta}{2e}}$ and we can rewrite Eqn. (13) as

$$\begin{aligned}\dot{V}(x) &\le -2(ce^{\frac{-\eta}{2e}} - \varsigma)|x| \\ &\le -2(ce^{\frac{-\eta}{2e}} - \varsigma)V(x)^{\frac{1}{2}}\end{aligned} , \tag{16}$$

where $\left(ce^{\frac{-\eta}{2e}} - \varsigma\right) > 0$. It means that all the solutions are starting from $V(x) \le 1$ and reach the equilibrium in a time period of $T_2 \le \frac{1}{\left(ce^{\frac{-\eta}{2e}} - \varsigma\right)}$. Finally, the dynamical system (10) achieves for the equilibrium in a fixed time $T(x_0) \le (T_1 + T_2)$.

***Proposition 1*:** In order to implement voltage regulation in the presence of both matched and mismatched perturbations, the control input can be assigned in the following manner:

$$u = u_{eq} + u_b , \tag{17}$$

where

$$u_{eq} = \varphi(z)|x_1|\left[x_2 + k_2 \operatorname{sgn}(s)\right] + \left(\frac{x_1}{LC}\right) + \left(\frac{x_2}{R_o C}\right) + \delta , \tag{18}$$

$$u_b = -k_1 |s|^{\frac{\eta_2 s^2}{1+\upsilon_2 s^2}} \operatorname{sgn}(s) , \tag{19}$$

$$\varphi(z) = \left(\frac{\beta\eta_1}{1+\upsilon_1 z^2}\right)\left[\frac{2x\ln(z)}{1+\upsilon_1 z^2}+1\right] z^{\frac{\eta_1 z^2}{1+\upsilon_1 z^2}+1} , \tag{20}$$

and $k_1 > 0$, $k_2 > 0$, $\eta_1 > 0$, $\upsilon_1 > 0$, and $\theta_2 = \frac{\eta_2}{1+\upsilon_2} > 1$.

The closed-loop controller outlined in Eqns. (17-20) is designed to ensure that the system reaches the equilibrium region stated in Eqn. (11)

$$T(x_0) \le \frac{1}{(k_1-\varsigma_3)(\theta_2-1)} + \frac{1}{\left(k_1 e^{\frac{-\eta_2}{2e}} - \varsigma_3\right)} + \frac{1}{(\beta-\varsigma_1)(\theta_1-1)} + \frac{1}{\left(\beta e^{\frac{-\eta_1}{2e}} - \varsigma_1\right)}$$

4 Matched and mismatched perturbations of nonlinear systems

This section discusses the development of a fixed-time sliding surface that guides the system toward the equilibrium trajectory, despite the occurrence of matched and mismatched disturbances.

Lemma 1: [4] This involves the analysis of a nonlinear second-order system that exhibits both matched and mismatched characteristics:

$$\begin{aligned}\dot{x}_1 &= x_2 + \sigma_1 \\ \dot{x}_2 &= f(x) + g(x)u + \sigma_2\end{aligned}. \qquad (21)$$

In the above relation, $x = (x_1, x_2) \in R^2$ and $u \in R$ are defined as the control inputs. Functions f and g are continuous functions with $f(0) \neq 0$ and $g(x) \neq 0$ for all $x \in R^2$. The term σ_1 represents a mismatched disturbance constrained by $|\sigma_1(t)| < \varsigma_1$, while σ_2 denotes a matched disturbance with $|\sigma_2(t)| < \varsigma_2$. In the absence of a controller capable of managing mismatched para-meters, the neighbourhood equilibrium set of system (21) is approximately $[0, -\sigma_1(t)]$. The sliding variable associated with the state-dependent variable exponent coefficient can be defined as follows:

$$s(x) = x_2 + \beta |x_1|^{\frac{\eta_1 x_1^2}{1+\upsilon_1 x_1^2}} sgn(x_1), \qquad (22)$$

where $x \in R$, $\eta_1 > 0$, $\upsilon_1 > 0$, $\theta = \frac{\eta_1}{1+\upsilon_1} > 1$ and $\beta > \varsigma_1 e^{\frac{\eta_1}{2e}}$. The closed-loop dynamical system is a robust, globally fixed-time stable system characterized by a steady state period within

$$\begin{aligned}T(x_0) \le &\frac{1}{(k_1 - \varsigma_3)(\theta_2 - 1)} + \frac{1}{k_1 e^{\frac{-\eta_2}{2e}} - \varsigma_3} \\ &+ \frac{1}{(\beta - \varsigma_1)(\theta_1 - 1)} + \frac{1}{\beta e^{\frac{-\eta_1}{2e}} - \varsigma_1}\end{aligned} \qquad (23)$$

where $k_1 > \varsigma_3 = \varsigma_2 + 2\beta\eta_1(1+\upsilon_1)(\varsigma_1 + k_2)$ and $k_2 > \varsigma_1$.

Lemma 2: [4] For $Z \ge 0$, we have $\varphi(z) > 0$ when $z > 1$, and $|\varphi(z)| \le 2\beta\eta_1(1 + \upsilon_1)$ when $0 \le z \le 1$.

***Proof*:** According to proposition 2 in [4], when $0 \le z \le 1$, we have

$$\varphi(z) = \frac{\beta\eta_1}{\left(1+\upsilon_1 z^2\right)^2}\left[2z\ln(z) + z + \upsilon_1 z^3\right] z^{\frac{\eta_1 z^2}{1+\upsilon_1 z^2}}. \qquad (24)$$

Note that $0 \le \frac{\beta\eta_1}{\left(1+\upsilon_1 z^2\right)^2} \le \beta\eta_1$ and $0 \le z^{\frac{\eta_1 z^2}{1+\upsilon_1 z^2}} \le 1$. From Eqn. (24), we establish the following relation for clarity:

$$\psi(z) = 2z\ln(z) + z + \upsilon_1 z^3. \qquad (25)$$

Differentiating (25) and setting it to 0 results in

$$\psi'(z) = 2\ln(z) + 3 + 3\upsilon_1 z^2 = 0. \qquad (26)$$

We observe that ψ decreases on the interval $(0, z_0)$ and increases on the interval $(z_0, 1)$. This leads to $|\psi(z)| \le \max\{1+\upsilon_1, |\psi(z_0)|\}$, and the result can be then calculated as

$$\psi(z_0) = -2z_0(1+\upsilon_1 z_0). \qquad (27)$$

Since $0 \le z \le 1$, the final result is obtained as $|\psi(z_0)| \le 2(1+\upsilon_1)$.

5 Controller design

Even when there are matched and unmatched disturbances, uncertainties, unmodeled characteristics, and noise. the state-dependent controller is designed to consistently track the reference signal. This work focuses on regulating the output voltage of a DC-DC converter. Consequently, Eqn. (6) allows for the following derivation.

Suppose that $x_1 = e = \overline{v_C} - v_r$, we have

$$\dot{x}_1 = \frac{\bar{i}_L}{C} - \frac{\overline{v_C}}{R_o C} + \sigma_1(t), \qquad (28)$$

where $\sigma_1(t) = \frac{\bar{v}_C}{R_o C} - \frac{\bar{v}_C}{RC}$ is assigned as the mismatched parameters.

Also let us define that $x_2 = \frac{\bar{i}_L}{C} - \frac{\bar{v}_C}{R_o C}$, then we have

$$\dot{x}_2 = \frac{\left(dv_{in} - v_r\right)}{LC} - \frac{x_1}{LC} - \frac{x_2}{R_o C} - \sigma_2(t), \qquad (29)$$

where $\sigma_2(t) = \left(1 - \frac{R_o}{R}\right)\left(\frac{\bar{v}_C}{R_o C}\right)$ is assigned as the mismatched parameters.

Based on Eqns. (28) and (29), the dynamic model of the DC-DC converter under mismatched perturbations can be expressed as:

$$\begin{aligned}\dot{x}_1 &= x_2 + \sigma_1(t)\\ \dot{x}_2 &= u - \frac{x_1}{LC} - \frac{x_2}{R_o C} - \sigma_2(t)\end{aligned}, \tag{30}$$

where $u = \dfrac{\left(dv_{in} - v_r\right)}{LC}$ is lumped as the state input.

6 Fixed-time stability proof

The block diagram of the proposed sliding surface with reaching law is shown in Fig. 4. By employing the sliding surface delineated in Eqn. (22), we can assert the following:

$$s = x_2 + \beta \left|x_1\right|^{\frac{\eta_1 x_1^2}{1+\upsilon_1 x_1^2}} \operatorname{sgn}(x_1)\ . \tag{31}$$

The derivative of Eqn. (31) yields

$$\dot{s} = u - \frac{x_1}{LC} - \frac{x_2}{R_o C} - \sigma_2(t) + \frac{\beta\eta_1 |x_1|(x_2+\sigma_1)}{1+\upsilon_1 x_1^2}\left(\frac{2\ln|x_1|}{1+\upsilon_1 x_1^2}+1\right)|x_1|^{\frac{\eta_1 x_1^2}{1+\upsilon_1 x_1^2}}\ . \tag{32}$$

Referring to *Proposition 1*, we will substitute the control signal u from Eqns. (17-19) into (32) and simplify the resulting expression:

$$\dot{s} = -k_1 |s|^{\frac{\eta_2 s^2}{1+\upsilon_2 s^2}} \operatorname{sgn}(s) + \delta - \sigma_2(t) + \varphi(z)|x_1|\left[\sigma_1 - k_2 \operatorname{sgn}(s)\right] \tag{33}$$

The derivative of the sliding surface is, in fact,

$$\dot{s} = -u_b + \delta - \sigma_2(t) - \varphi(z,\sigma_1,k_2)\ . \tag{34}$$

The Lyapunov candidate function is defined as

$$V = s^2. \tag{35}$$

The derivative of this function with trajectory (33) reveals two different cases. It is evidently clear that

$$\dot{V}(s) \le 2|s|\left\{-k_1 |s|^{\frac{\eta_2 s^2}{1+\upsilon_2 s^2}} + \delta - \sigma_2(t) + \varphi(z)|x_1|\left[\operatorname{sgn}(s)\sigma_1 - k_2\right]\right\}. \tag{36}$$

For the first case, when $|x_1| > 1$, we find that $\varphi(z)|x_1| > 0$. Therefore,

$$\dot{V}(s) \le 2|s|\left[-k_1 |s|^{\frac{\eta_2 s^2}{1+\upsilon_2 s^2}} + \varsigma_2 + \varphi(z)|x_1|\left(\varsigma_1 - k_2\right)\right]. \tag{37}$$

By assumption in *Lemma 2*, we know that $k_2 > \varsigma_1$, then we have $\varphi(z)|x_1|(\varsigma_1 - k_2) < 0$. We can rewrite Eqn. (37) as a simple expression as:

$$\dot{V}(s) \le 2|s|\left(-k_1 |s|^{\frac{\eta_2 s^2}{1+\upsilon_2 s^2}} + \varsigma_2\right). \tag{38}$$

For the second case, when $|x_1| \le 1$, and referring to *Lemma 2*, we have $|\varphi(z)|x_1|| \le 2\beta\eta_1(1+\upsilon_1)$. Then Eqn. (37) can be written as:

$$\dot{V}(s) \le 2|s|\left(-k_1 |s|^{\frac{\eta_2 s^2}{1+\upsilon_2 s^2}} + \varsigma_3\right), \tag{39}$$

where
$$\varsigma_3 = \varsigma_2 + 2\beta\eta_1(1+\upsilon_1)\left(\varsigma_1 + k_2\right). \tag{40}$$

Application of *Theorem 1* demonstrates that the closed-loop dynamical system described in (33), starting at initial surface $s(0) = s_0$, will achieve $s = 0$ within a fixed time satisfying

$$T(s_0) \le \frac{1}{(k_1 - \varsigma_3)(\theta_2 - 1)} + \frac{1}{\left(k_1 e^{\frac{-\eta_2}{2e}} - \varsigma_3\right)}.$$

According to Eqn. (31), when the sliding surface $s = 0$, it follows that

$$\dot{x}_1 = -\beta |x_1|^{\frac{\eta_1 x_1^2}{1+\upsilon_1 x_1^2}} \operatorname{sgn}(x_1) + \sigma_1\ . \tag{41}$$

We observe that $x_1(t)$ starts at $x_1(0) = x_{10}$ and reaches equilibrium within a fixed time satisfying

$$T(x_{10}) \le \frac{1}{(\beta - \varsigma_1)(\theta_1 - 1)} + \frac{1}{\left(\beta e^{\frac{-\eta_1}{2e}} - \varsigma_1\right)}.$$

With *Theorem 2*, we determine that $x_2(t)$ tracks $-\sigma_1(t)$ over a fixed-time period. Accordingly, we obtain a fixed-time estimator for the mismatched disturbance without utilizing observers. By substituting the control signals from Eqns. (17-19) into (32), the dynamical system reaches the equilibrium region in a fixed time satisfying the condition $T(x_0) \le T(s_0) + T(x_{10})$.

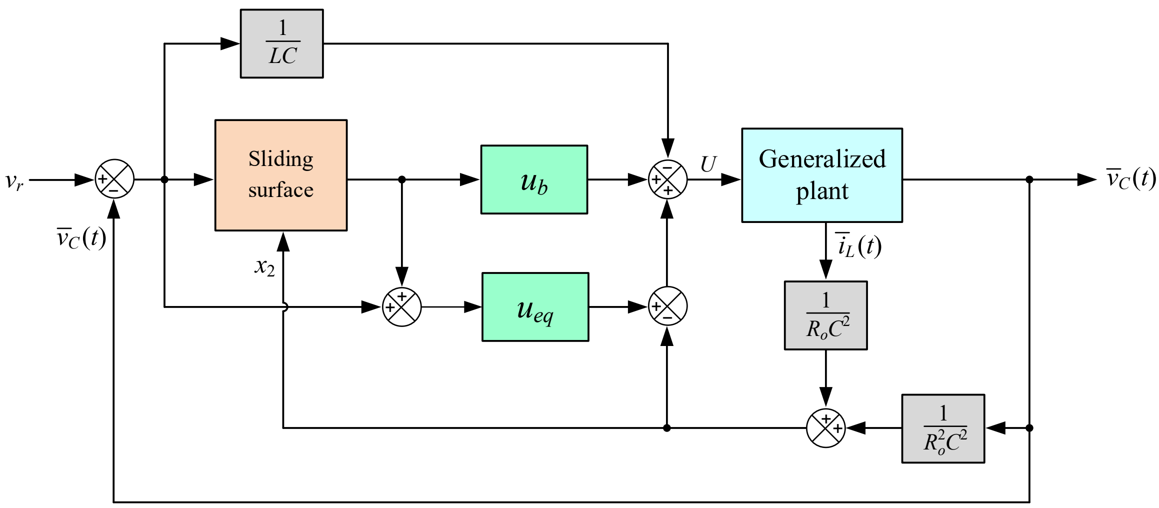

Fig. 4. Block diagram of the proposed sliding mode control system

7 Simulation results

The system depicted in Fig. 1 has been simulated using both a conventional proportional-integral (PI) controller and the proposed fixed-time SMC in MATALB. The buck converter parameters were set as follows: $v_{in} = 30$ V, $R = 6.71\ \Omega$, $L = 40$ mH, and $C = 4\ \mu$F. Step references (v_r) of 10 V, 25 V, and 15 V were used to evaluate tracking performance under both matched and mismatched perturbations.

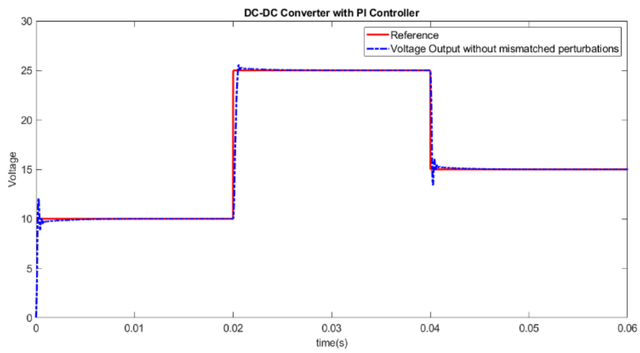

(a)

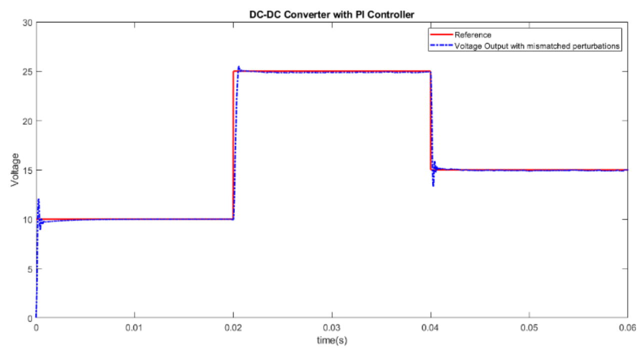

(b)

Fig. 5. Output voltage of the DC-DC converter using PI controller: (a) without mismatched perturbations, (b) with mismatched perturbations

Figure 5 shows the simulated output voltage of the system controlled by a PI controller with parameters set at $K_p = 200$ and $K_i = 0.5$. As illustrated in Fig. 5(a), the PI controller demonstrates generally effective performance; however, it is noted that overshoot occurs during instances of speed variation. Ultimately, the PI controller is capable of driving the system toward the setpoint without any steady-state error. Nonetheless, when parameters are mismatched, the PI controller can still function in this situation. However, there will be some voltage error during speed changes and the steady-state period. As can be observed from Fig. 5(b), the PI controller needs a few second to recover the system to a state of zero error.

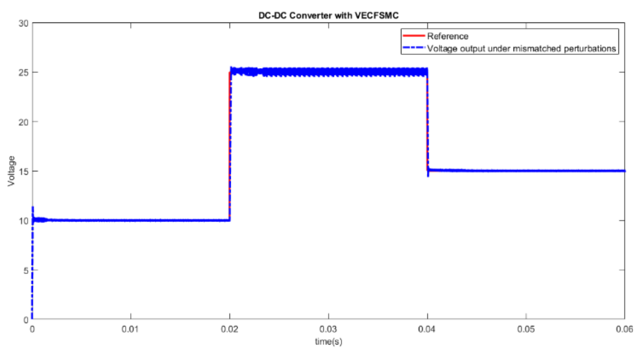

Fig. 6. Output voltage of the DC-DC converter using the proposed fixed-time SMC under mismatched perturbations

Figure 6 shows the output voltage of the DC-DC converter using the proposed fixed-time SMC in Fig. 4. The perturbation terms are defined as:

$\sigma_1(t) = 0.1 - 0.2 \sin (0.4t)$,

$\sigma_2(t) = 0.2 \sin (t) - 0.4 \sin (3t)$.

The configuration of the controller parameters follows the guidelines outlined in [4]. As a result, the selected parameters are recommended to satisfy the conditions:

$\varsigma_1 \geq \sigma_1$, $\varsigma_2 \geq \sigma_2$, and k_1, $k_2 > \varsigma_3$.

To ensure that

$$\theta = \frac{\eta_1}{1+\upsilon_1} > 1 \text{ and } \beta > \varsigma_1 e^{\frac{\eta_1}{2e}},$$

the parameters η_1 and υ_1 must be greater than zero ($\eta_1 > 0$ and $\upsilon_1 > 0$). The specific parameters are defined as follows: $k_1 = k_2 = 2$, $\eta_1 = 1.2$, $\upsilon_1 = 1$, $\eta_2 = 4$, $\upsilon_2 = 1$, $\varsigma_1 = 0.3$, $\varsigma_2 = 0.6$, and $\beta = 5.5$. The system demonstrates exceptional performance in tracking voltage commands without any overshoot. There is no steady-state error during the voltage change or the steady-state period. The response is faster than that of a PI controller. However, the output voltage exhibits some chattering due to the high switching function. The system is not only stable and resilient but also consistently provides power to the load.

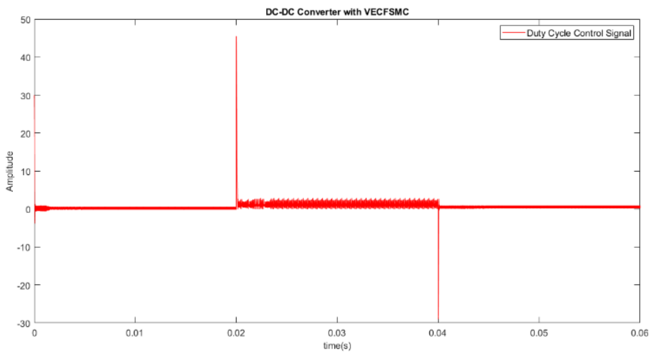

Fig. 7. Duty cycle control signal of the proposed fixed-time SMC

Figure 7 illustrates the corresponding duty cycle signal generated by the controller. While high-frequency switching allows for accurate tracking, it also introduces some chattering, which is a common issue in SMC. This minor limitation can be addressed in future work by exploring continuous sliding mode approaches or boundary layer techniques to minimize switching activity.

In summary, the proposed fixed-time SMC clearly outperforms the PI controller, particularly in speed, robustness, and accuracy. Its simple structure, observer-free design, and strong disturbance rejection capabilities make it an effective and practical solution for voltage regulation in DC-DC converters operating under uncertain conditions.

8 Conclusions

This paper presents a variable exponent coefficient sliding surface designed to control the output voltage of a DC-DC converter, addressing both matched and mismatched disturbances in the mathematical model. It considers the dynamic model of the converter, incorporating uncertainties and lumped load disturbances. The conventional PI controller was employed to regulate the output voltage and exhibited excellent performance in the absence of mismatched disturbances. Nevertheless, it demonstrates certain distortion in the voltage output when confronted with mismatched parameters. The fixed-time sliding mode control method, utilizing a variable exponent coefficient and functioning without an observer, efficiently regulates voltage and mitigates both matched and mismatched disturbances. A stability proof is presented for the fixed-time sliding controller. The proposed variable exponent coefficient sliding mode controller offers a simple solution for voltage regulation, requiring only a few parameters. This fixed-time variable exponent coefficient approach is more straightforward compared to other finite or fixed-time methods, making it suitable for real-world applications. The proposed controller shows a strong response without requiring an observer; however, it exhibits chattering when compared to the linear control method. Future work may explore more sophisticated sliding surfaces and reaching laws to reduce chattering. Additionally, it is important to note that as mathematical complexity increases, the challenges associated with implementation also increase.

Acknowledgement

This work was supported by School of Engineering, King Mongkut's Institute of Technology Ladkrabang (KMITL). The authors are deeply indebted to the anonymous reviewers for their helpful comments and suggestions.

References

[1] F. Mumtaz, N. Z. Yahaya, S. T. Meraj, B. Singh, R. Kannan, and O. Ibrahim, "Review on non-isolated DC-DC converters and their control techniques for renewable energy application," *Ain Shams Engineering Journal,* vol. 12, no. 4, pp. 3747-3763, 2021.

[2] L. G. Wu, J. Liu, S. Vazquez, and S. K. Mazumder, "Sliding mode control in power converters and drives: A review," *IEEE/CAA Journal of Automatica Sinica*, vol. 9, no. 3, pp. 392–406, 2022.

[3] A. Polyakov, "Nonlinear feedback design for fixed-time stabilization of linear control systems," *IEEE Transactions on Automatic Control*, vol. 57, no. 8, pp. 2106-2110, 2012.

[4] E. Moulay, V. Léchappé, E. Bernuau, M. Defoort, and F. Plestan, "Fixed-time sliding mode control with mismatched disturbances," *Automatica*, vol. 136, no. 4, 110009, 2022.

[5] F. Yacef, N. Rizoug, L. Degaa, O. Bouhali, and M. Hamerlain, "Extended state observer-based adaptive fuzzy tracking control for a quadrotor UAV," *2018 5th International Conference on Control, Decision and Information Technologies (CoDIT'18)*, Thessaloniki, Greece, April 10-13, pp. 1023–1028, 2018.

[6] A. K. Junejo, W. Xu, C. Mu, M. M. Ismail, and Y. Liu, "Adaptive speed control of PMSM drive system based a new sliding-mode reaching law," *IEEE Transactions on Power Electronics,* vol. 35, no. 11, pp. 12110–12121, 2020.

[7] W. Xu, A. K. Junejo, Y. Liu, and Md. R. Islam, "Improved continuous fast terminal sliding mode control with extended state observer for speed regulation of PMSM drive system," *IEEE Transaction on Vehicular Technology*, vol. 68, no.11, pp. 10465–10476, 2019.

[8] Y. C. Liu, S. Laghrouche, D. Depernet, A. N'diaye, A. Djerdir, and M. Cirrincione, "Super-twisting sliding-mode observer-based model reference adaptive speed control of PMSM drives," *Journal of the Franklin Institute*, vol. 360, no. 2, pp. 985–1004, 2023.

[9] V. Cholahan, N. Wongvanich, W Tangsrirat, "Robust constant exponent coefficient fixed-time control based on finite-time extended sliding mode observer of permanent magnet synchronous motors," *Energies*, vol. 16, no. 21, 7454, 2023.

[10] H. Choi, "LMI-Based sliding surface design for integral sliding mode control of mismatched uncertain systems," *IEEE Transaction on Automatic Control,* vol. 42, no. 4, pp. 736-742, 2007.

[11] C. C. Wen, and C. C. Cheng, "Design of sliding mode for mismatched uncertain systems to achieve asymptotical stability," *Journal of the Franklin Institute*, vol. 345, no. 8, pp. 926–941, 2008.

[12] Y. Wang, and M. Chen, "Fixed-time disturbance observer-based sliding mode control for mismatched uncertain systems," *International Journal of Control, Automation and Systems*, vol. 20, pp. 2792–2804, 2022.

[13] J. Li, Y. Yang, C. Hua and X. Guan, "Fixed-time backstepping control design for high-order strict-feedback non-linear systems via terminal sliding mode," *IET Control Theory & Applications*, vol. 11, no. 8, pp. 1184-1193, 2017.

[14] J. Li, S. Wang, L. Zhang, S. Li, "Nonlinear cascade sliding mode control based on extended state observer method for a DC-DC buck converter: Design and hardware experimentation," *Proceedings of the Institution of Mechanical Engineers, Part I: Journal of Systems and Control Engineering*, vol. 237, no. 4, pp. 608-621, 2022.

[15] W. Shuwang, S. Li, J. Su, J. Li, and L. Zhang. "Extended state observer-based nonsingular terminal sliding mode controller for a DC-DC buck converter with disturbances: Theoretical analysis and experimental verification." *International Journal of Control,* vol. 96, no. 7, pp. 1661–71, 2022.

[16] S. Huerta-Moro, O. Martínez-Fuentes, V. R. Gonzalez-Diaz, and E. Tlelo-Cuautle, "On the sliding mode control applied to a DC-DC buck converter," *Technologies,* vol. 11, no. 33, 2023.

[17] E. Moulay, V. Léchappé, E. Bernuau, and F. Plestan, "Robust fixed-time stability: Application to sliding mode control," *IEEE Transaction on Automatic Control,* vol. 67, no. 2, pp. 1061-1066, 2022.

Varin Cholahan obtained his B. Eng. degree in Mechanical Engineering (Control Systems) from the Faculty of Engineering at Mahanakorn University of Technology (MUT), Bangkok, Thailand, in 2002. He is presently pursuing a D. Eng. degree in Electrical Engineering at the School of Engineering, King Mongkut's Institute of Technology Ladkrabang (KMITL), Bangkok, Thailand. His research interests are focused on control systems.

Worapong Tangsrirat received his B. Ind. Tech. degree (Honors) in Electronics Engineering, and M. Eng. and D. Eng. degrees in Electrical Engineering, all from the Faculty of Engineering, King Mongkut's Institute of Technology Ladkrabang (KMITL), Bangkok, Thailand, in 1991, 1997, and 2003, respectively. His research interests are primarily in the areas of analog signal processing and integrated circuits, current-mode circuits, active filter and oscillator design, electronic instrumentation and control systems, and chaotic synchronization and control. He has edited or written 15 books and has published more than 150 research articles in many peer-reviewed international journals. Prof. Tangsrirat has accomplished a note-worthy milestone by consistently ranking in the "Top 2% List of the World's Scientists", both in terms of research impact for the career-long achievement and the most recent single year 2023.

Received 21 May 2025